nature geoscience
SUPPLEMENTARY INFORMATION
DOI: 10.1038/NGEO2986
In the format provided by the authors and unedited.

Reduced North American terrestrial primary productivity linked to anomalous Arctic warming

Jin-Soo Kim[1], Jong-Seong Kug[1,*], Su-Jong Jeong[2,*] Deborah N. Huntzinger[3], Anna M. Michalak[4], Christopher R. Schwalm[5,6], Yaxing Wei[7] and Kevin Schaefer[8]

[1] Division of Environmental Science and Engineering, Pohang University of Science and Technology (POSTECH), Pohang, South Korea
[2] School of Environmental Science and Engineering, South University of Science and Technology of China (SUSTECH), Shenzhen, China
[3]School of Earth Sciences and Environmental Sustainability, Northern Arizona University, Flagstaff, Arizona 86011, USA.
[4]Department of Global Ecology, Carnegie Institution for Science, Stanford, California 94305, USA.
[5]Woods Hole Research Center, Falmouth, Massachusetts 02540, USA.
[6]Center for Ecosystem Science and Society, Northern Arizona University, Flagstaff Arizona 86011, USA.
[7]Environmental Sciences Division and Climate Change Science Institute, Oak Ridge National Laboratory, Oak Ridge, Tennessee 37831, USA.
[8]National Snow and Ice Data Center, Cooperative Institute for Research in Environmental Sciences, University of Colorado at Boulder, Boulder, Colorado 80309, USA

*Corresponding authors. Email: jskug@postech.ac.kr and sujong@sustc.edu.cn

Sensitivity Analyses

The Arctic temperature-induced teleconnection, such as temperature and precipitation, affects terrestrial productivity over the most of North America, but terrestrial responses would be different depending on land cover, plant type, and region. In this regard, multiple regression approach was used in this study to investigate the individual contributions of the temperature and precipitation anomalies[1,2] for both of data- and process-driven GPP as shown in Supplementary Fig. 8 and 9 as using Eq. 1.

$$\delta(GPP) = \frac{\partial(\mathrm{GPP})}{\partial(\mathrm{Temp})}\delta(\mathrm{Temp}) + \frac{\partial(\mathrm{GPP})}{\partial(\mathrm{Prec})}\delta(\mathrm{Prec}) + \varepsilon$$

$$= \gamma_{\mathrm{GPP}}^{\mathrm{Temp}}\delta\mathrm{Temp} + \gamma_{\mathrm{GPP}}^{\mathrm{Prec}}\delta\mathrm{Prec} + \varepsilon, \qquad (1)$$

where $\gamma_{\mathrm{GPP}}^{\mathrm{Temp}}$ and $\gamma_{\mathrm{GPP}}^{\mathrm{Prec}}$ are obtained from the coefficients using the partial regression method; these parameters approximately represent the sensitivities of GPP to surface temperature (Supplementary Fig. 8a,c and 9a,c) and precipitation (Supplementary Fig. 8b,d and 9b,d), respectively. As a result, the northern part of North America has relatively high sensitivity of GPP to temperature as temperature-limited ecosystems, while sensitivity of GPP to precipitation shows significant signal in the southwestern United States as water-limited ecosystems. Interestingly, anomalous Arctic warming-induced teleconnection has negative temperature anomalies over the northern part of North America and negative precipitation anomalies over the southwestern United States. This in-phase relationship between GPP sensitivity to atmospheric anomalies and Arctic-induced atmospheric anomalies amplify Arctic warming impacts on terrestrial response over North America. It can be written as follows:

$$\frac{\mathrm{d(GPP)}}{\mathrm{d(ART)}} = \frac{\partial(\mathrm{GPP})}{\partial(\mathrm{Temp})}\frac{\mathrm{d(Temp)}}{\mathrm{d(ART)}} + \frac{\partial(\mathrm{GPP})}{\partial(\mathrm{Prec})}\frac{\mathrm{d(Prec)}}{\mathrm{d(ART)}} + \varepsilon$$

$$\gamma_{GPP}^{ART} = \gamma_{GPP}^{Temp}\gamma_{Temp}^{ART} + \gamma_{GPP}^{Prec}\gamma_{Prec}^{ART} + \varepsilon \quad (2)$$

where γ_{GPP}^{ART} is GPP anomalies with respect to the ART index. Likewise, γ_{Temp}^{ART} and γ_{Prec}^{ART} are temperature and precipitation anomalies with respect to the ART index as shown in Fig. 1c,d, respectively.

This sensitivity analysis can be applied to future changes in Arctic-induced GPP anomalies by comparing historical and RCP4.5 scenario in the CMIP5 ESMs. Based on Eq. 2, the future changes in GPP responses to the Arctic temperature variation ($\Delta\gamma_{GPP}^{ART}$) can be separated by four terms as follows:

$$\Delta\gamma_{GPP}^{ART} = \Delta\gamma_{GPP}^{Temp}\gamma_{Temp}^{ART} + \Delta\gamma_{Temp}^{ART}\gamma_{GPP}^{Temp} + \Delta\gamma_{GPP}^{Prec}\gamma_{Prec}^{ART} + \Delta\gamma_{Prec}^{ART}\gamma_{GPP}^{Prec} \quad (3)$$

Consequently, enhanced GPP response to the Arctic temperature variation in future projection (Supplementary Fig. 10) would be explained by enhanced sensitivity of GPP to local temperature under greenhouse warming (Supplementary Fig. 11). This is consistent with several previous studies that argued stronger sensitivity of terrestrial response to local temperature variation under greenhouse warming[3–7].

Supplementary References

1. Piao, S. *et al*. Evaluation of terrestrial carbon cycle models for their response to climate variability and to CO_2 trends. *Global Change Biology*. **19,** 2117–2132 (2013).

2. Kim, J. S., Kug, J. S., Yoon, J. H. & Jeong, S. J. Increased atmospheric CO_2 growth rate during El Niño driven by reduced terrestrial productivity in the CMIP5 ESMs. *J. Clim*. **29**, 8783–8805 (2016).

3. Gu, L. *et al*., The 2007 eastern US spring freezes: Increased cold damage in a warming world? *Bioscience* **58,** 253–262 (2008).

4. Rigby, J. R. & Porporato, A. Spring frost risk in a changing climate. *Geophys*. *Res*. *Lett*. **35,** L12703 (2008).

5. Augspurger, C. K. Spring 2007 warmth and frost: phenology, damage and refoliation in a temperate deciduous forest. *Funct Ecol* **23,** 1031–1039 (2009).

6. Augspurger, C. K. Reconstructing patterns of temperature, phenology, and frost damage over 124 years: Spring damage risk is increasing. *Ecology* **94,** 41–50 (2013).

7. Liu, Y. W. *et al.* Changes in interannual climate sensitivities of terrestrial carbon fluxes during the 21st century predicted by CMIP5 Earth System Models. *J*. *Geophys*. *Res*. **121**, 903–918 (2016).

8. Wei, Y. et al. The North American Carbon Program Multi-scale synthesis and Terrestrial Model Intercomparison Project–Part 2: environmental driver data. *Geosci*. *Model*. *Dev*. **6,** 5375–5422 (2013).

9. Rayner, A. *et al*. Global analyses of sea surface temperature, sea ice, and night marine air temperature since the late nineteenth century. *J*. *Geophys*. *Res*. **108,** 4407 (2003).

Supplementary Table 1 | Lagged autocorrelation values for the ART index

Correlation	Lag +1 month	Lag +2 month
Jan	0.04	0.08
Feb	−0.11	−0.00
Mar	0.37*	0.38*
Apr	0.48*	0.33*
May	0.35*	0.11
Jun	0.55*	0.28
Jul	0.44*	0.23
Aug	0.64*	0.45*
Sep	0.67*	0.28
Oct	0.33*	−0.03
Nov	0.24	0.07
Dec	0.07	−0.10

*****indicates significance at the 95% confidence level on the basis of a Student's *t*-test.

Supplementary Table 2 | Used periods of each dataset

Data	Affiliation	Spatial resolution	Period
HadCRUT4	University of York	5° × 5°	1979–2015
ERA-Interim	European Centre for Medium-Range Weather Forecasts Reanalysis	1.5° × 1.5°	1979–2015
Climatic Research Unit	University of East Anglia	0.5° × 0.5°	1979–2014
Hadley Centre Sea Ice	Met Office Hadley Centre	1° × 1°	1979–2015
NDVI	NASA Ames Ecological Forecasting Lab	0.5° × 0.5° (re-gridded)	1982–2013
MTE GPP	Max Planck Institute for biogeochemistry	0.5° × 0.5°	1982–2011
MsTMIP	North American Carbon Program	0.5° × 0.5°	1979–2010
Earth System Model	Coupled Model Intercomparison Project Phase 5	2.5° × 2.5° (re-gridded)	1976–2005 (historical), 2070–2099 (RCP 4.5)

Supplementary Table 3 | MsTMIP models used in this study

Model name	Affiliation	Nitrogen cycling included[1]
Biome-BGC	NASA Ames	Yes
CLASS-CTEM-N	McMaster University	Yes
CLM4	Oak Ridge National Lab	Yes
CLM4VIC	Pacific Northwest National Lab	Yes
DLEM	Auburn University	Yes
GTEC	Oak Ridge National Lab	No
ISAM	University of Illinois Urbana Champaign	Yes
LPJ-wsl	Laboratoire des Sciences du Climat et l'Environnement, France	No
ORCHIDEE-LSCE	Laboratoire des Sciences du Climat et de l'Environnement, France	No
SiB3	NASA Jet Propulsion Laboratory	No
SiBCASA	National Snow and Ice Data Center	No
TEM6	Oak Ridge National Laboratory	Yes
TRIPLEX-GHG	University of Quebec at Montreal	Yes
VEGAS2.1	University of Maryland	No
VISIT	National Institute for Environ. Studies, Japan	No

[1]Models use North American Regional Reanalysis (NARR) and CRU-NCEP climate forcing, time-varying land-use history, and atmospheric CO_2 concentration; however, nitrogen cycling simulations are different for each model[8].

Supplementary Table 4 | CMIP5 ESMs used in this study

Model Name	Modeling Center (or Group)
BNU-ESM	College of Global Change and Earth System Science, Beijing Normal University
CCSM4	National Center for Atmospheric Research
CESM1-BGC	Community Earth System Model Contributors
CESM1-CAM5	
CESM1-WACCM	
CanESM2	Canadian Centre for Climate Modelling and Analysis
GFDL-ESM2M	NOAA Geophysical Fluid Dynamics Laboratory
GISS-E2-H-CC	NASA Goddard Institute for Space Studies
GISS-E2-H	
GISS-E2-R-CC	
GISS-E2-R	
HadGEM2-CC	Met Office Hadley Centre
HadGEM2-ES	
IPSL-CM5A-LR	Institute Pierre Simon Laplace
IPSL-CM5A-MR	
IPSL-CM5B-LR	
MIROC-ESM-CHEM	Japan Agency for Marine-Earth Science and Technology, Atmosphere and Ocean Research Institute (The University of Tokyo), and National Institute for Environmental Studies
MIROC-ESM	
MPI-ESM-LR	Max Planck Institute for Meteorology
MPI-ESM-MR	
NorESM1-ME	Norwegian Climate Centre
NorESM1-M	
bcc-csm1-1-m	Beijing Climate Center, China Meteorological Administration
bcc-csm1-1	
inmcm4	Institute of Numerical Mathematics, Russian Academy of Sciences

Supplementary Table 5 | Ameriflux sites used in this study

Site	Latitude	Longitude	Vegetation type	Year	Reference doi	Anomalous Arctic warming	Anomalous Arctic cooling
US-MMS (Morgan Monroe State Forest)	39.32	−86.41	Deciduous Broadleaf Forests	1999 – 2014	10.17190/AMF/1246080	2002, 2003, 2005, 2011, 2013, 2014	1999, 2000, 2001, 2004, 2006, 2007, 2008, 2009, 2010, 2012
US-UMB (Univ. of Mich. Biological Station)	45.56	−84.71	Deciduous Broadleaf Forests	2000 – 2014	10.17190/AMF/1246107	2002, 2003, 2011, 2013, 2014	2000, 2001, 2004, 2005, 2006, 2007, 2008, 2009, 2010, 2012
US-Ha1 (Harvard Forest EMS Tower)	42.54	−72.17	Deciduous Broadleaf Forests	1991 – 2012	10.17190/AMF/1246059	1995, 1996, 1997, 1998, 2000, 2002, 2003, 2004, 2005, 2011	1991, 1992, 1993, 1994, 1999, 2001, 2006, 2007, 2008, 2009, 2010, 2012
US-NR1 (Niwot Ridge Forest)	40.03	−105.55	Evergreen Needleleaf Forests	1998 – 2014	10.17190/AMF/1246088	2002, 2003, 2005, 2011, 2013, 2014	1999, 2000, 2001, 2004, 2006, 2007, 2008, 2009, 2010, 2012
US-Ne1 (Mead-irrigated continuous maize site)	41.17	−96.48	Croplands	2001 – 2013	10.17190/AMF/1246084	2002, 2003, 2011, 2013	2001, 2004, 2005, 2006, 2007, 2008, 2009,
US-Ne2 (Irrigated	41.16	−96.47	Croplands		10.17190/AMF/1246085		

maize–soybean rotation site)							2010, 2012
US-Ne3 (Rainfed maize–soybean rotation site)	41.18	−96.44	Croplands		10.17190/AMF/1246086		
US-ARM (ARM Southern Great Plains site-Lamont)	36.61	−97.49	Croplands	2003–2012	10.17190/AMF/1246027	2003, 2005, 2011	2004, 2006, 2007, 2008, 2009, 2010, 2012
US-Los (Lost Creek)	46.08	−89.98	Permanent Wetlands	2000–2014	10.17190/AMF/1246071	2002, 2003, 2011	2000, 2001, 2004, 2005, 2006, 2007, 2008, 2009, 2010

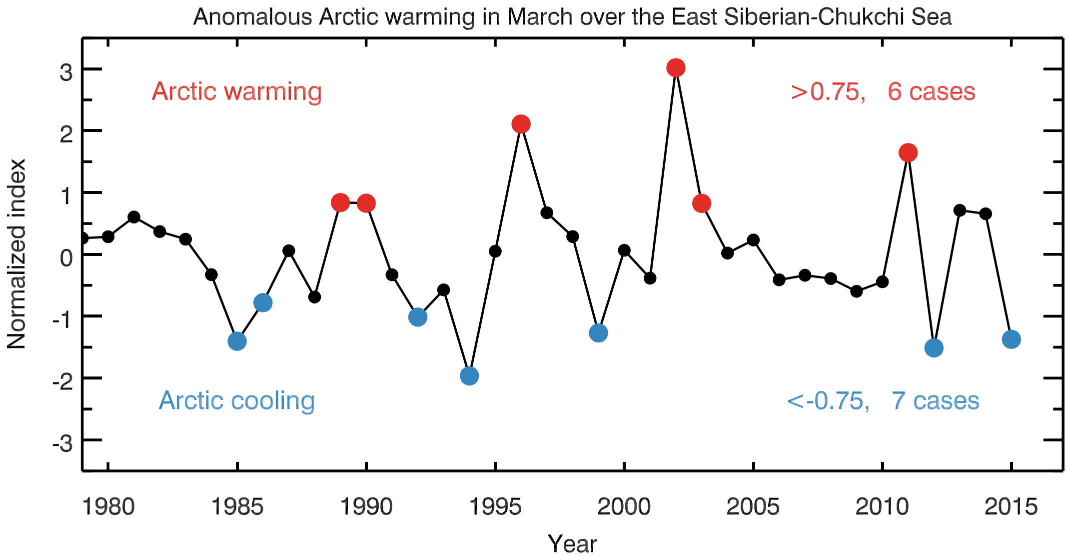

Supplementary Figure 1 | Time series of Normalized March Arctic temperature. Anomalous Arctic warming in March over the East Siberian–Chukchi Sea (160° E–160° W, 65°–80° N) for the period 1979–2015. Red and blue dots indicate >0.75σ and <−0.75σ years of Arctic temperature anomaly, respectively.

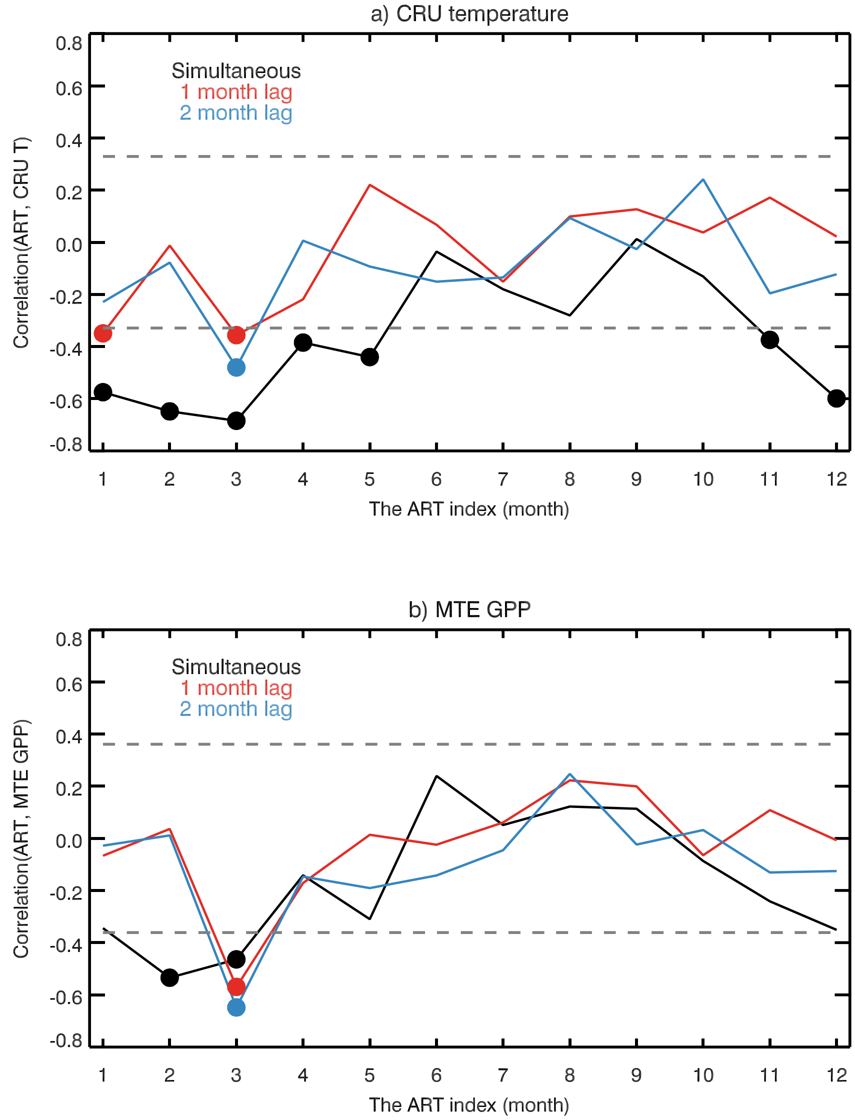

Supplementary Figure 2 | Relationship between anomalous Arctic warming and anomalies over North America. a, b, Correlation coefficients between anomalous Arctic warming over the East Siberian–Chukchi Sea (160° E–160° W, 65°–80° N), i.e., ART index, and temperature anomaly (**a**) and MTE GPP (**b**) over North America (125°–85° W, 30°–60° N). Black, red, blue lines show correlations for simultaneous, 1 month lag, and 2 month lag, respectively. For example, blue line in March is a correlation coefficient between the March ART index and temperature anomaly over North America in May. Dashed lines indicate the significant criteria at the 95% confidence level (calculated using a Student's *t*-test) and filled circle shows significant correlation values.

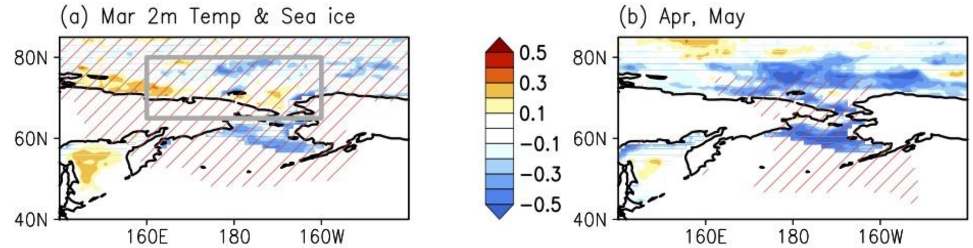

Supplementary Figure 3 | Relationship between surface temperature and sea-ice over the East Siberian–Chukchi Sea. a, b, Correlation coefficients of sea-ice concentration, provided by Hadley Centre Sea Ice data for the period 1979–2015[9] (http://www.metoffice.gov.uk/hadobs/hadisst), in March (**a**) and April–May (**b**) with respect to the Arctic temperature (ART) index based on the March surface temperature in the East Siberian–Chukchi Sea (gray box; 160° E–160° W, 65°–80° N). Hatching indicates significant regions for 2-m temperature anomalies at the 95% confidence level based on a Student's *t*-test.

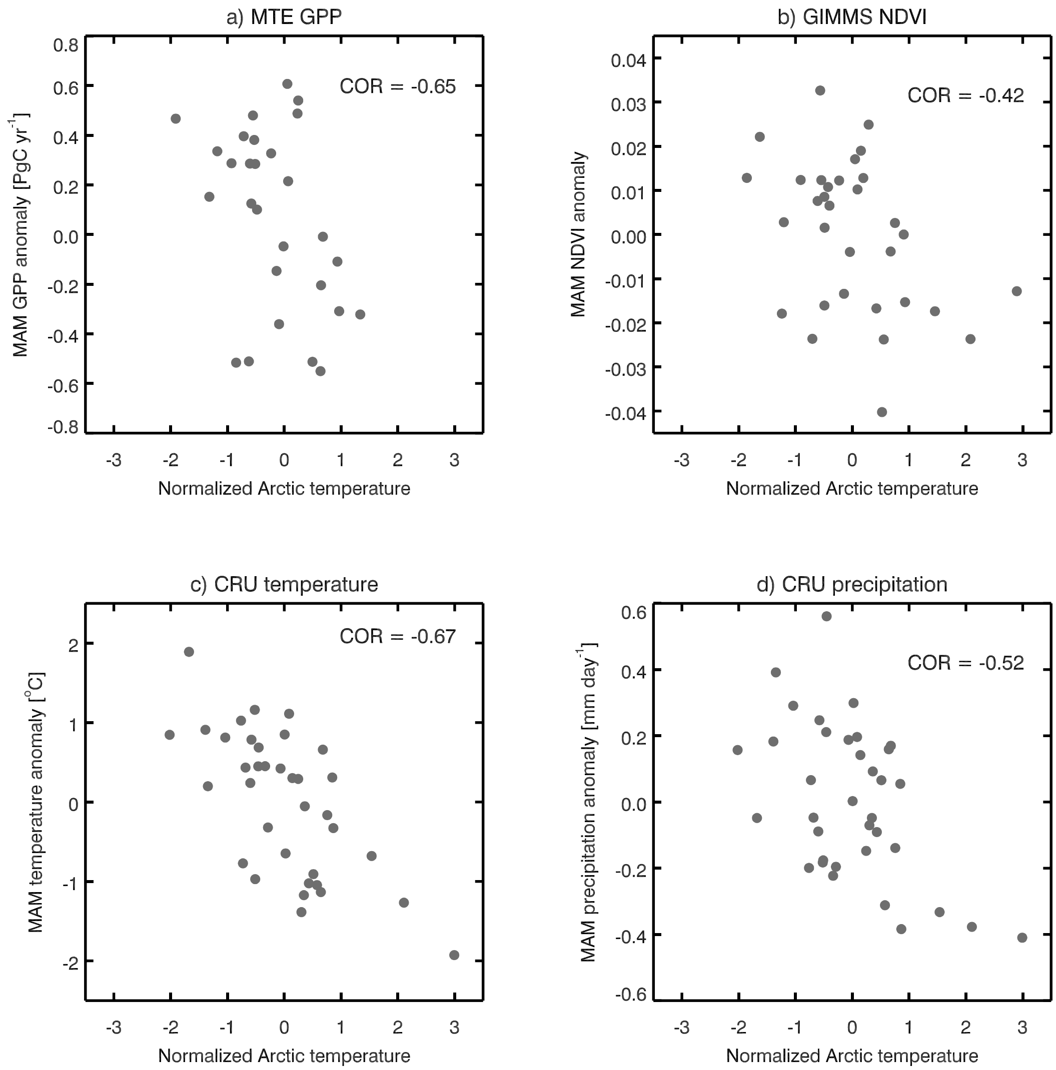

Supplementary Figure 4 | Scatter plot of spring season anomaly over North America and normalized Arctic temperature anomaly. a–d, The normalized Arctic temperature anomaly versus March–May mean MTE GPP (**a**), GIMMS NDVI (**b**), temperature (**c**) over North America (125°–85° W, 30°–60° N), and precipitation (**d**) over South Central United States (110°–100° W, 32°–38° N).

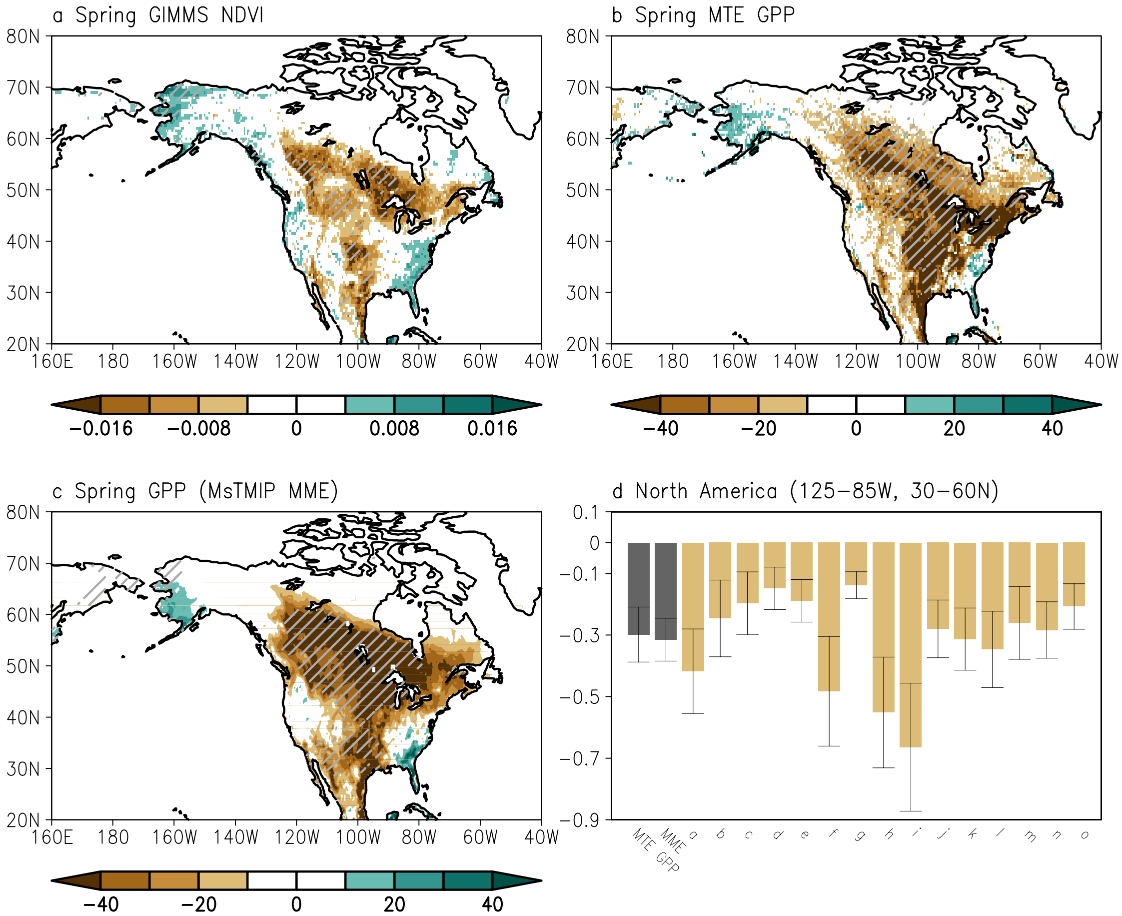

Supplementary Figure 5 | Arctic warming impacts on spring terrestrial productivity. a–c, Regression coefficients of the spring (March–May) Global Inventory Modeling and Mapping Studies NDVI (**a**), flux tower data-driven GPP from the Max Planck Institute for biogeochemistry (gC m^{-2} yr^{-1}) (**b**), and MME simulated GPP based on the Multi-scale Synthesis and Terrestrial Model Intercomparison Project (MsTMIP) (gC m^{-2} yr^{-1}) (**c**) with respect to the ART index for the period 1982–2010 that common period of data sets while Fig. 2 is based on available period for each data set. Hatching denotes local significance at the 95% confidence level on the basis of a Student's *t*-test. **d,** Regression coefficient of the total GPP over North America (125°–85° 420 W, 30°–60° N) with respect to the ART index based on individual models (PgC yr−1). The scale bars represent a range of 95% confidence levels from internal variability based on a Student's t-test.

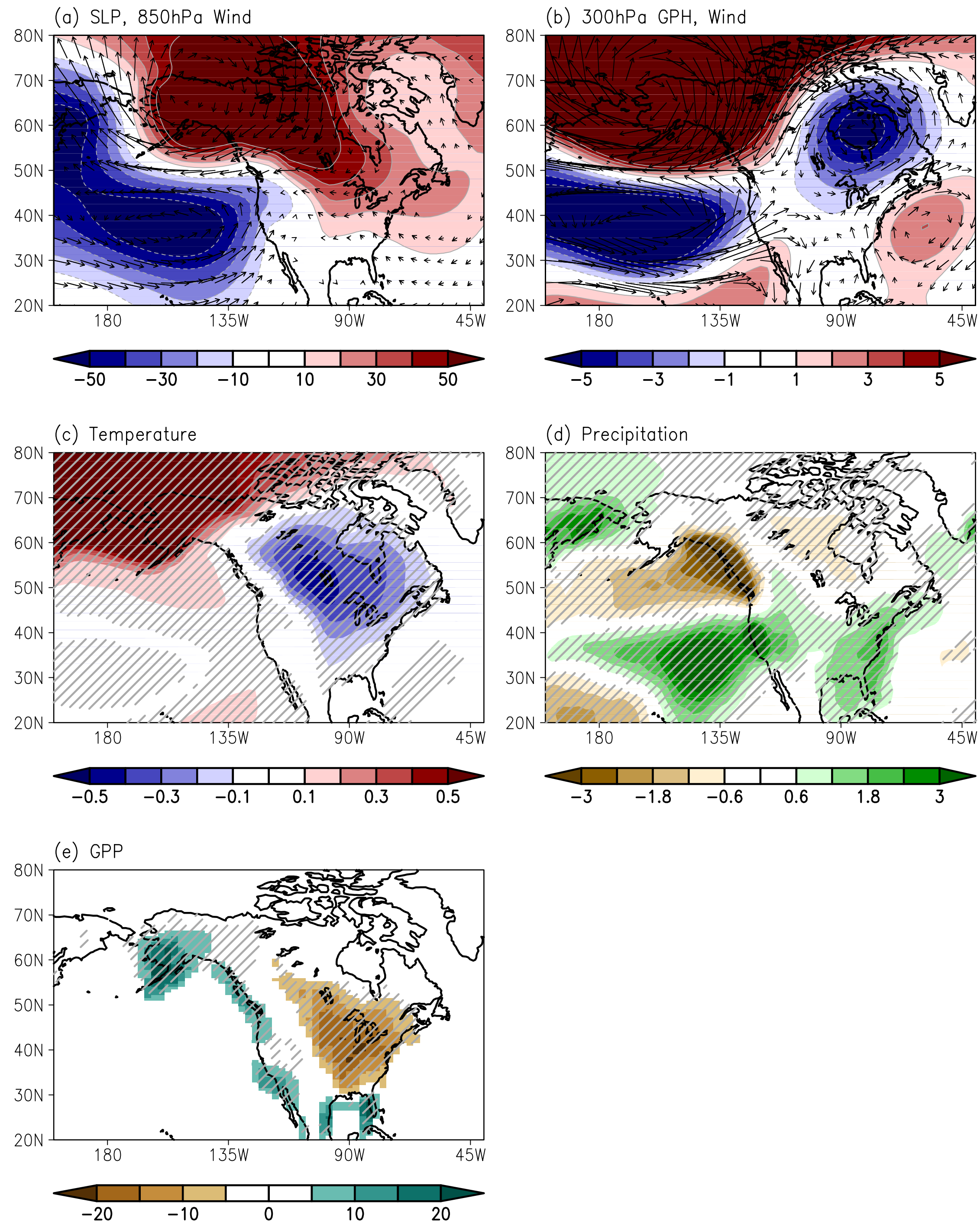

Supplementary Figure 6 | Arctic temperature-induced teleconnection in the CMIP5 historical experiment. a–e, MME regression coefficients of March–May mean sea-level pressure (Pa), 850-hPa wind (**a**), 300-hPa geopotential height (m) and wind (**b**), surface temperature (K) (**c**), precipitation (mm day^{-1}) (**d**), and GPP (gC m^{-2} yr^{-1}) (**e**) with respect to the March ART index based on 25 ESMs in the historical experiment. Hatching denotes local significance at the 95% confidence level based on a Student's *t*-test. The

CMIP5 ESMs simulate atmospheric teleconnection related to anomalous Arctic warming to a certain degree, but temperature anomalies over the northern part of North America relatively small to the observational result as shown in Fig. 1. Also, precipitation anomalies pattern shows significant positive anomalies over east and west coastal region in the United State; however, negative signal in the South Central United State does not represent in the ESMs in contrast to observational result. This bias would be related to underestimation of GPP anomalies with respect to the ART index.

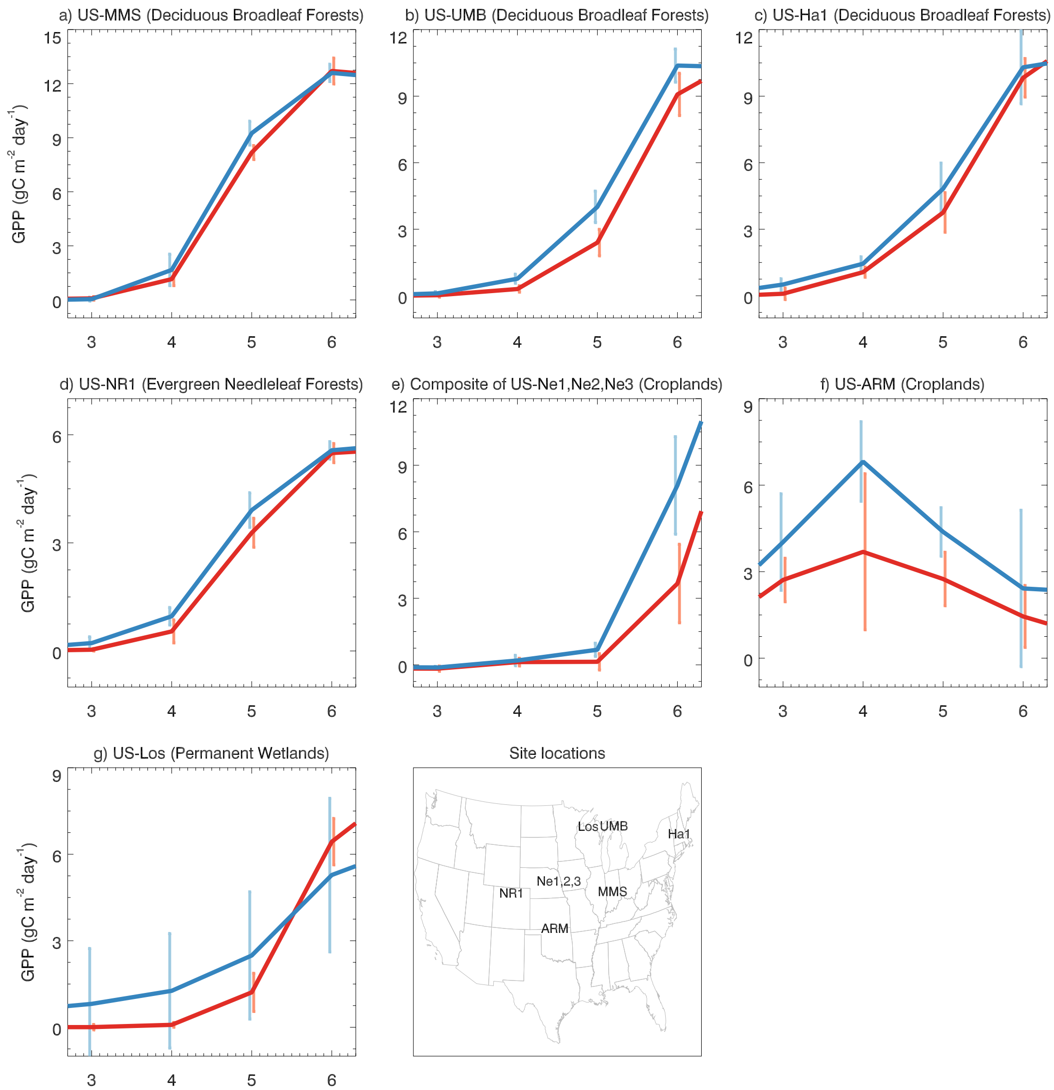

Supplementary Figure 7 | Flux tower GPP for the cases of Arctic warming and cooling. a–f, Composite of monthly GPP (gC m^{-1} day^{-1}) in individual flux towers in the cases of Arctic warming (red) and cooling (blue). Error bars indicate 95% confidence levels. US-MMS (**a**), US-UMB (**b**), US-Ha1 (**c**), US-NR1 (**d**), composite of US-Ne1, Ne2, and Ne3 (**e**), US-ARM (**f**), and US-Los (**g**) are used to obtain composites in the cases of Arctic warming and cooling. As each site has different periods of data availability, Arctic warming and cooling events are defined by ART anomalies for each period for which data are available. Site locations are marked on the map.

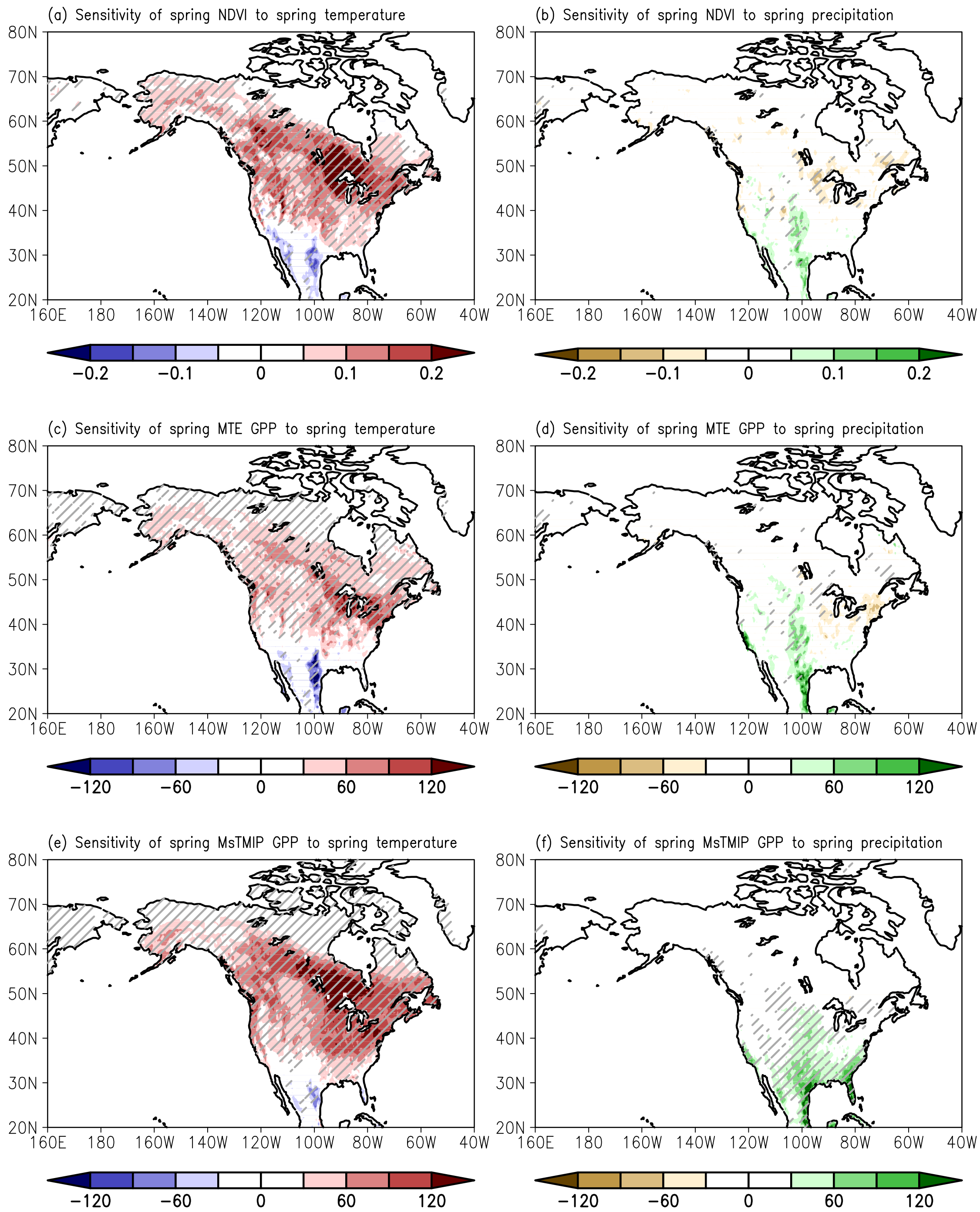

Supplementary Figure 8 | Sensitivity of spring terrestrial productivity to local spring temperature and precipitation. a–f, Partial regression coefficients of spring (March–May) NDVI (**a**, **b**), data-driven GPP (**c**, **d**), and MME MsTMIP GPP (**e**, **f**) (gC m^{-2} yr^{-1}) with respect to spring temperature and precipitation based on CRU TS3.23. Hatching denotes local significance at the 95% confidence level based on a Student's *t*-test.

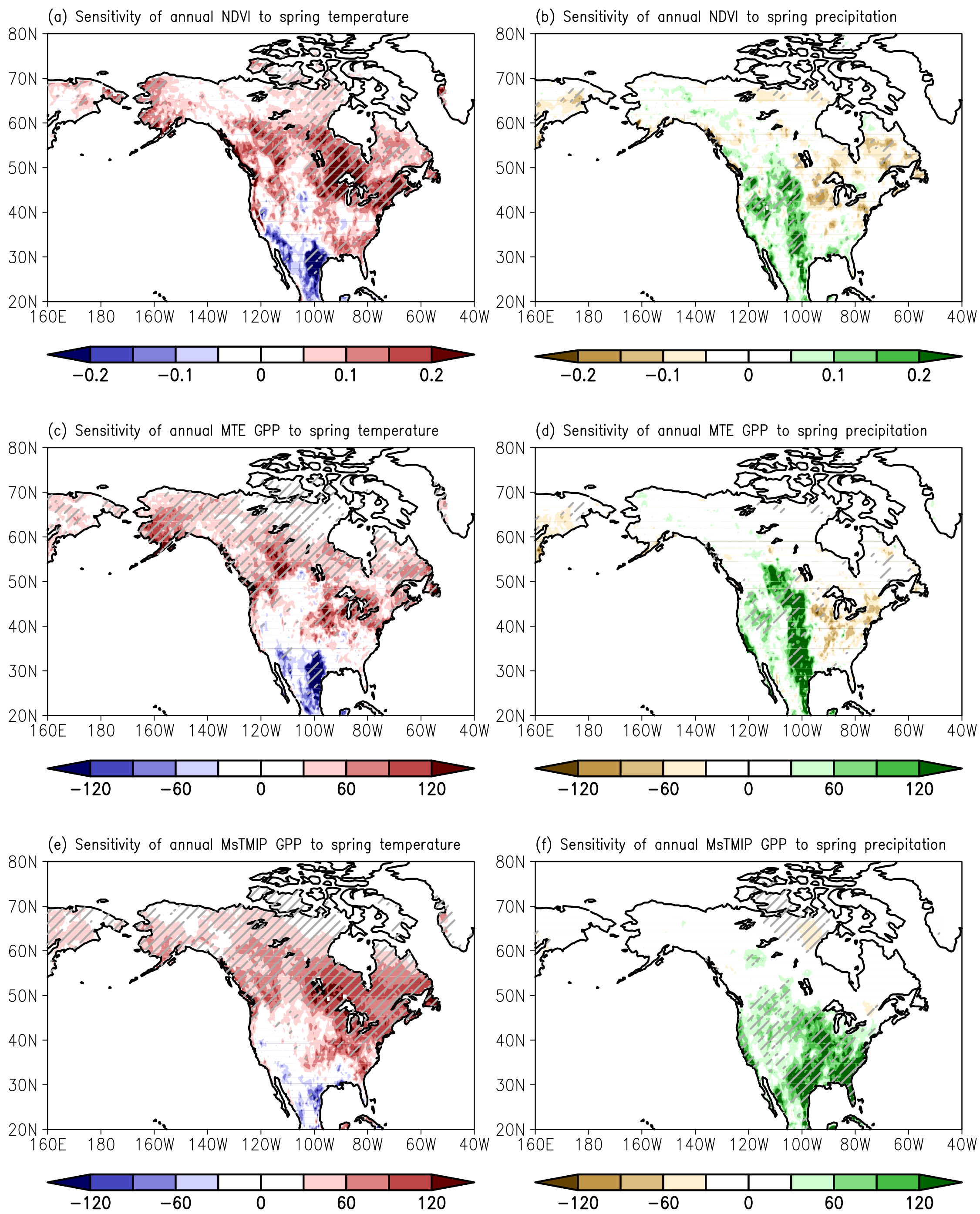

Supplementary Figure 9 | Sensitivity of annual terrestrial productivity to local spring temperature and precipitation. a–f, Partial regression coefficients of annual (Jan–Dec) NDVI (**a**, **b**), data-driven GPP, and MME MsTMIP GPP (**e**, **f**) (gC m^{-2} yr^{-1}) (**c**, **d**) with respect to spring (March–May) temperature and precipitation based on CRU TS3.23. Hatching denotes local significance at the 95% confidence level based on a Student's *t*-test.

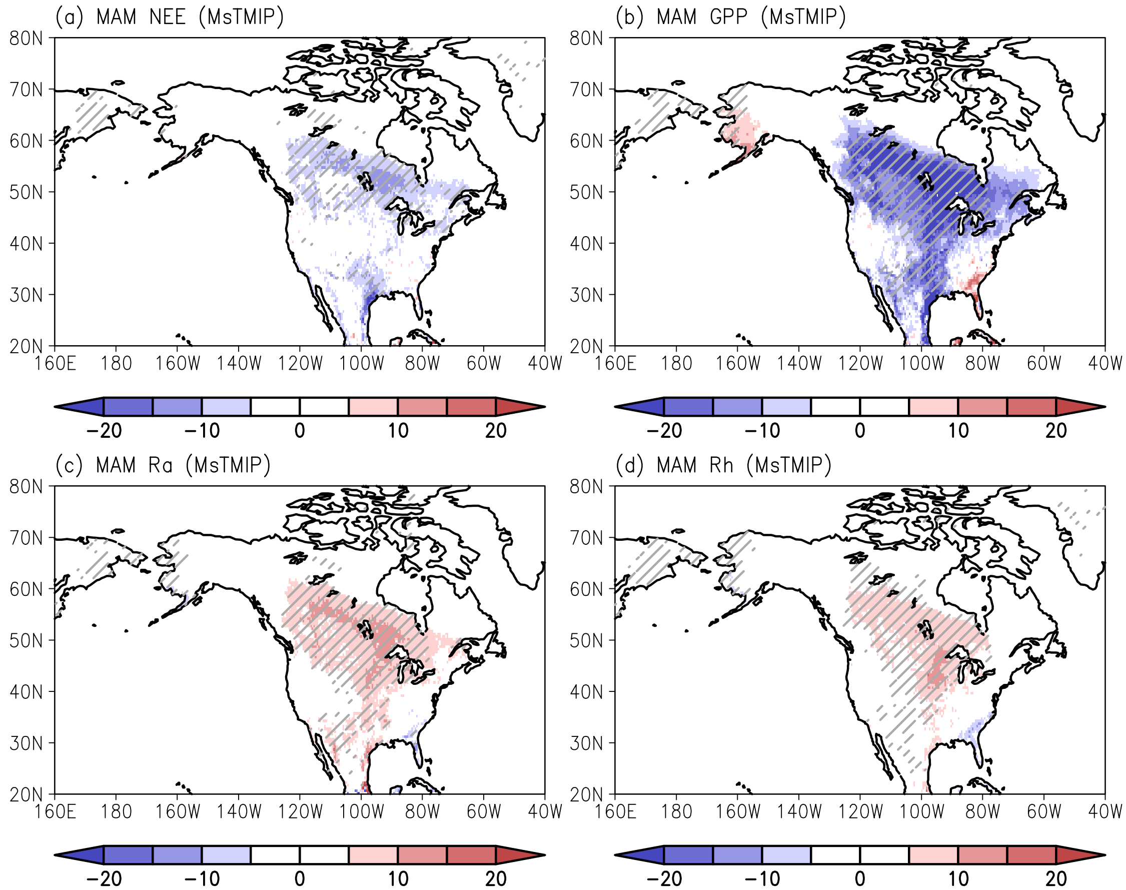

Supplementary Figure 10 | Arctic warming impacts on terrestrial processes. a–d, Regression coefficients of the spring (March–May) MME simulated NEE (**a**), GPP (**b**), R_a (**c**), and R_h (**d**) based on the Multi-scale Synthesis and Terrestrial Model Intercomparison Project (MsTMIP) (gC m^{-2} yr^{-1}) with respect to the ART index. Hatching denotes local significance at the 95% confidence level on the basis of a Student’s *t*-test.

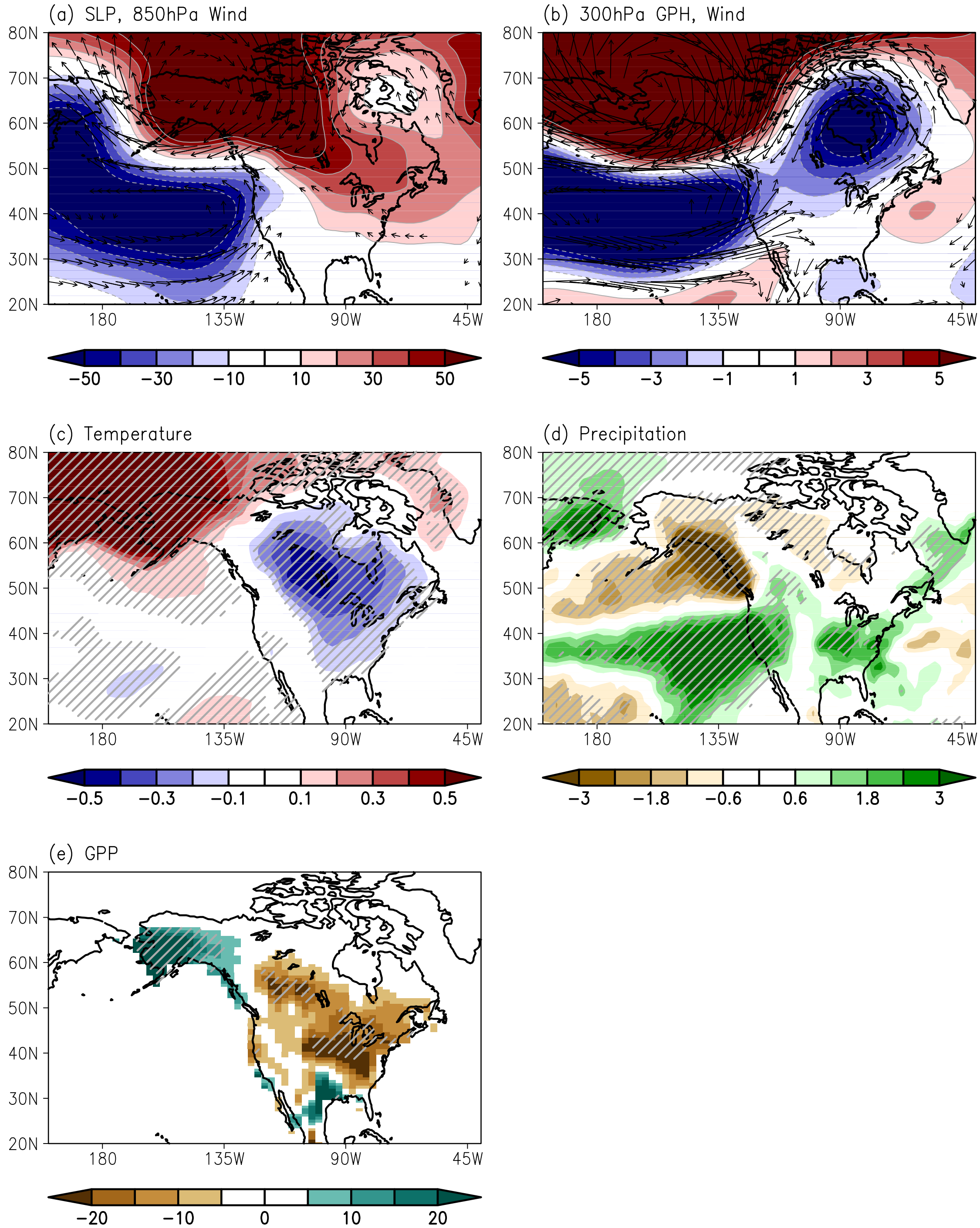

Supplementary Figure 11 | Arctic temperature-induced teleconnection in the CMIP5 future projection. a–e, MME regression coefficients of March–May mean sea-level pressure (Pa), 850-hPa wind (**a**), 300-hPa geopotential height (m) and wind (**b**), surface temperature (K) (**c**), precipitation (mm day^{-1}) (**d**), and GPP (gC m^{-2} yr^{-1}) (**e**) with respect to the ART index based on 25 Earth System Models in the RCP4.5 experiment. Hatching denotes local significance at the 95% confidence level based on a Student's *t*-test.

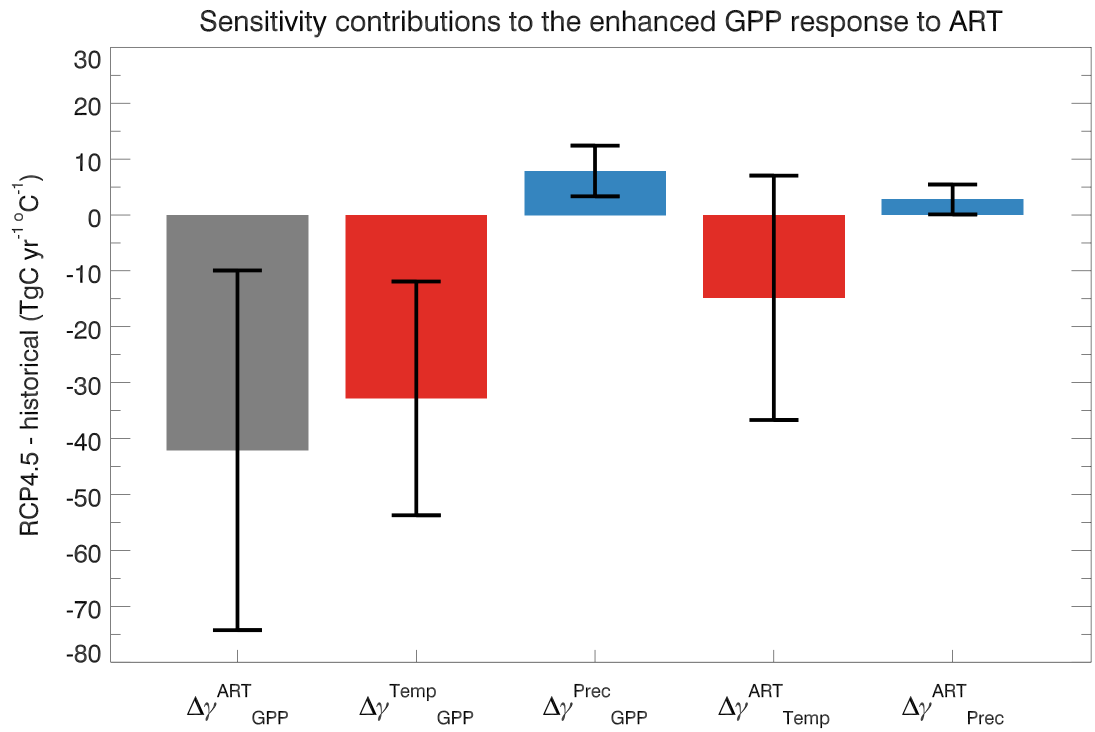

Supplementary Figure 12 | Sensitivity contributions to the enhanced GPP response to Arctic temperature variation. Gray bar indicates differences in the regression coefficients of MAM GPP anomalies over North America (125°–85° W, 30°–60° N) with respect to the ART index between the historical (1976–2005) and RCP4.5 (2070–2099) scenario ($\Delta\gamma^{ART}_{GPP}$). The others indicate each term in Eq. 3 that are contribution to future changes in the GPP sensitivity to temperature ($\Delta\gamma^{Temp}_{GPP}\gamma^{ART}_{Temp}$) and precipitation ($\Delta\gamma^{Prec}_{GPP}\gamma^{ART}_{Prec}$), and future changes in the temperature ($\Delta\gamma^{ART}_{Temp}\gamma^{Temp}_{GPP}$) and precipitation anomalies ($\Delta\gamma^{ART}_{Prec}\gamma^{Prec}_{GPP}$) with respect to Arctic temperature variation. Each bar shows the MME results and error bars indicate 95% confidence levels based on the Student's *t*-test.